Chirality dependent carbon nanotube interactions

A. Popescu, L. M. Woods, and I. V. Bondarev

Phys. Rev. B **83**, 081406 — Published 14 February 2011

DOI: 10.1103/PhysRevB.83.081406

Chirality Dependent Carbon Nanotube Interactions

A. Popescu[1], L. M. Woods[1], and I. V. Bondarev[2]

[1]*Department of Physics, University of South Florida, Tampa, Florida 33620*

[2]*Physics Department, North Carolina Central University, Durham, North Carolina 27707*

The interaction between two concentric carbon nanotubes is studied using a quantum electrodynamical approach which includes the absorptive and dispersive properties via the chirality dependent dielectric response functions for each carbon nanotube. It is found that at tube separations similar to their equilibrium distances, the interaction is dominated by the collective excitations in the electron energy loss spectra originating from interband transitions. The existence of strong low frequency transitions peaks from both tubes and their overlap are responsible for their stronger interaction. Nanotube chiralities possessing such collective excitation features are found to have the strongest interaction.

Carbon nanotubes (CNTs) are quasi-one dimensional (1D) hollow wires consisting of one (single wall) or more (multi wall) rolled graphene sheets into cylinders[1]. The specific way of rolling is characterized by a chirality index (*n*,*m*), and determines the CNT electronic structure. The inter-tube interaction is of long ranged dispersive nature and its understanding is important in tailoring the properties of various CNT complexes. It is also important for experimental realization of new effects and devices recently proposed, such as trapping of cold atoms[2] and their entanglement[3] near CNTs, exciton-plasmon coupling[4], surface profiling and nanolithography applications[5].

Various mechanisms may be responsible for governing the CNT interactions. It is known that geometrical factors such as nanotube separation and the π-stacking patterns[6] are important. At the same time, the collective surface excitations in terms of each CNT dielectric response also have a profound effect on their mutual interaction; however their specific functionalities have not been qualitatively and quantitatively understood yet. Since CNTs of virtually the same radial size can possess different

electronic properties, investigating their interactions presents a unique opportunity to obtain insight into specific dielectric response features affecting the force between metallic and semiconducting cylindrical surfaces. Potentially this can also help unveil the role of collective excitations in the energetic stability of CNTs of various chiral combinations.

CNTs interact with each other via the long ranged Casimir force induced by quantum electromagnetic fluctuations. The Casimir force is quantum mechanical and relativistic in its nature, and it has been studied extensively since the prediction of the existence of an attraction between neutral mirrors in vacuum[7]. After the first report of observation of this spectacular effect[8], new measurements with improved accuracy have been done involving different geometries[9]. The Casimir force has also been considered theoretically with methods primarily based on the zero-point summation approach and Lifshitz theory[10,11]. Since the Lifshitz theory cannot be applied to geometries other than parallel plates, researchers have used the Proximity Force Approximation (PFA) to estimate the interaction between CNTs[12,13]. The method is based on approximating the curved surfaces at very close distances by a series of parallel plates and summing their energies. Thus, the PFA is inherently an additive approach, applicable to objects at very close separations (still to be greater than the objects inter-atomic distances) under the assumption that the CNT dielectric response is the same as the one for the plates.

In this Letter, we consider the interaction between two concentric cylindrical graphene sheets using a quantum electrodynamical (QED) approach suitable for dispersing and absorbing media[14]. The method allows taking into account the full CNT cylindrical geometry by solving the Fourier-domain operator Maxwell equations with appropriate boundary conditions and including their particular dielectric functions. The dielectric functions are calculated beforehand based on the quasi-1D energy band structure of each CNT. It is found that at relatively small inter-tube separations the collective interband excitations have a profound effect on their mutual interaction. Thus, the chiralities of concentric graphene sheets with similar radial sizes exhibiting these features may be responsible for the most

preferred CNT pairs. Furthermore, our results seem to be in agreement with experimental measurements on determining the chirality of individual double wall CNTs[6].

The system is modeled by two infinitely long, infinitely thin, continuous concentric cylinders immersed in vacuum (see Fig.1). Atomistic calculations have shown that the thin shell approximation is fairly reasonable up to an error $\sim (a_{CC}/R)^3$ with a_{CC} being the carbon-carbon distance and R – the nanotube radius[15]. Previous studies of CNT interactions based on the PFA-Lifshitz theory have also demonstrated the applicability of this assumption for distances larger than a few times a_{CC}[16]. Thus here we consider that CNTs can be represented as infinitely thin cylinders. Further, each cylinder is characterized by the nanotube complex dynamic axial dielectric function $\varepsilon_{zz}(\boldsymbol{R}_{1,2},\omega)$ with the z-direction along the CNT axis. The CNT azimuthal and radial dielectric tensor components are neglected, since the transverse response is known to be much smaller [17]. Experimental and theoretical studies show that the suppression of the transverse dielectric response arise from the cylindrical anisotropy of the system and the strong transverse dipolarization effects, and results in the CNT transparency for EM radiation polarized perpendicular to the nanotube axis[17,18].

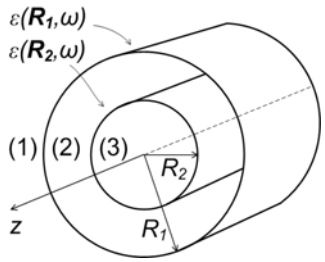

FIG. 1. Schematics of concentric CNTs in vacuum. The nanotube radii are R_1 and R_2 and the vacuum permittivity and permeability are ε_0 and μ_0, respectively. The regions limited by the CNT surfaces are denoted as (1), (2), (3).

The QED approach we employ here is a macroscopic theory. It was applied previously with success for distances larger than the carbon-carbon atomic separations to study near-field electromagnetic (EM) effects in pristine[4] and hybrid CNTs with near-surface atomic states present[19]. The quantization scheme generates the second-quantized Hamiltonian $\hat{H} = \sum_{i=1,2}\int_0^\infty d\omega \hbar\omega \int d\boldsymbol{R}_i \hat{f}^+(\boldsymbol{R}_i,\omega)\hat{f}(\boldsymbol{R}_i,\omega)$ of the vacuum/CNT assisted EM field, with the bosonic operators $\hat{f}^+$ ($\hat{f}$) creating (annihilating) surface

electromagnetic excitations of frequency ω at points $\boldsymbol{R}_{1,2} = (R_{1,2}, \varphi_{1,2}, z_{1,2})$. The Fourier-domain electric field operator at an arbitrary point $\boldsymbol{r} = (r, \varphi, z)$ is given by $\hat{\boldsymbol{E}}(\boldsymbol{r}, \omega) = i\omega\mu_0 \sum_{i=1,2} \int d\boldsymbol{R}_i \boldsymbol{G}(\boldsymbol{r}, \boldsymbol{R}_i, \omega) \cdot \hat{\boldsymbol{J}}(\boldsymbol{R}_i, \omega)$, where $\boldsymbol{G}(\boldsymbol{r}, \boldsymbol{R}_i, \omega)$ is the dyadic EM field Green's function (GF), and $\hat{\boldsymbol{J}}(\boldsymbol{R}_i, \omega) = \left[\omega/(\mu_0 c^2)\right]\left[\hbar \operatorname{Im} \varepsilon_{zz}(\boldsymbol{R}_i, \omega)/(\pi\varepsilon_0)\right]^{1/2} \hat{\boldsymbol{f}}(\boldsymbol{R}_i, \omega)\boldsymbol{e}_z$ is the surface current density operator selected in such a way as to ensure the correct QED equal-time commutation relations for the electric and magnetic field operators[14]. $\boldsymbol{e}_z$ is the unit vector along the CNT axis; ε_0, μ_0 and c are the dielectric constant, magnetic permeability and vacuum speed of light, respectively.

The dyadic GF satisfies the wave equation

$$\nabla \times \nabla \times \boldsymbol{G}(\boldsymbol{r}, \boldsymbol{r}', \omega) - \frac{\omega^2}{c^2} \boldsymbol{G}(\boldsymbol{r}, \boldsymbol{r}', \omega) = \delta(\boldsymbol{r} - \boldsymbol{r}')\boldsymbol{I} \tag{1}$$

where $\boldsymbol{I}$ is the unit tensor. It can further be decomposed as $\boldsymbol{G}^{(fs)} = \boldsymbol{G}^{(0)}\delta_{fs} + \boldsymbol{G}^{(fs)}_{scatt}$ with $\boldsymbol{G}^{(0)}$ and $\boldsymbol{G}^{(fs)}_{scatt}$ representing the contributions of the direct and scattered waves[20], respectively, with a point-like field source located in region (s) and the field registered in region (f) (see Fig.1). The boundary conditions for Eq. (1) are obtained from the ones for the electric and magnetic field components on the CNT surfaces[2,19]

$$\boldsymbol{e}_r \times \left[\boldsymbol{G}(\boldsymbol{r}, \boldsymbol{r}', \omega)\big|_{R_{1,2}^+} - \boldsymbol{G}(\boldsymbol{r}, \boldsymbol{r}', \omega)\big|_{R_{1,2}^-}\right] = 0 \tag{2}$$

$$\boldsymbol{e}_r \times \nabla \times \left[\boldsymbol{G}(\boldsymbol{r}, \boldsymbol{r}', \omega)\big|_{R_{1,2}^+} - \boldsymbol{G}(\boldsymbol{r}, \boldsymbol{r}', \omega)\big|_{R_{1,2}^-}\right] = i\omega\mu_0 \boldsymbol{\sigma}^{(1,2)}(\boldsymbol{r}, \omega) \cdot \boldsymbol{G}(\boldsymbol{r}, \boldsymbol{r}', \omega)\big|_{R_{1,2}} \tag{3}$$

where $\boldsymbol{e}_r$ is the unit vector along the radial direction. The discontinuity in Eq. (3) results from the full account of the finite absorption and dispersion for both CNTs by means of their conductivity tensors approximated by their largest components $\sigma_{zz}^{(1,2)}(\boldsymbol{R}_{1,2}, \omega) = -i\omega\varepsilon_0\left[\varepsilon_{zz}(\boldsymbol{R}_{1,2}, \omega) - 1\right]/(S\rho_T)$, with S being the CNT surface area, and ρ_T - the cubic density of the tubule. Following the procedure described in Ref. [20], we expand $\boldsymbol{G}^{(0)}$ and $\boldsymbol{G}^{(fs)}_{scatt}$ into series of even and odd vector cylindrical functions with unknown coefficients to be found from Eqs. (2) and (3). This splits the EM modes in the system into TE

and TM polarizations. Eqs. (2) and (3) yield a set of 32 equations (16 for each polarization) with 32 unknown coefficients., which we solve algebraically.

Using the expressions for the electric and magnetic fields, the EM stress tensor is constructed[14,21]

$$\boldsymbol{T}(\boldsymbol{r},\boldsymbol{r}') = \boldsymbol{T}_1(\boldsymbol{r},\boldsymbol{r}') + \boldsymbol{T}_2(\boldsymbol{r},\boldsymbol{r}') - \frac{1}{2}\boldsymbol{I}Tr\left[\boldsymbol{T}_1(\boldsymbol{r},\boldsymbol{r}') + \boldsymbol{T}_2(\boldsymbol{r},\boldsymbol{r}')\right] \tag{4}$$

$$\boldsymbol{T}_1(\boldsymbol{r},\boldsymbol{r}') = \frac{\hbar}{\pi}\int_0^\infty d\omega \frac{\omega^2}{c^2}\,\mathrm{Im}\left[\boldsymbol{G}(\boldsymbol{r},\boldsymbol{r}',\omega)\right] \tag{5}$$

$$\boldsymbol{T}_2(\boldsymbol{r},\boldsymbol{r}') = -\frac{\hbar}{\pi}\int_0^\infty d\omega\,\mathrm{Im}\left[\nabla\times\boldsymbol{G}(\boldsymbol{r},\boldsymbol{r}',\omega)\times\overleftarrow{\nabla}'\right] \tag{6}$$

We are interested in the radial component $\boldsymbol{T}_{rr}$ which describes the radiation pressure of the virtual EM field on each CNT surface in the system. The force per unit area exerted on the tubes surfaces is given by[14]

$$F_i = \lim_{r\to R_i}\left\{\lim_{\boldsymbol{r}'\to\boldsymbol{r}}\left(\boldsymbol{T}_{rr}^{(i)}(\boldsymbol{r},\boldsymbol{r}') - \boldsymbol{T}_{rr}^{(i+1)}(\boldsymbol{r},\boldsymbol{r}')\right)\right\}, i = 1,2 \tag{7}$$

$F_{1,2}$ found from Eq. (7) are of equal magnitude and opposite direction indicating attraction between the cylindrical surfaces. The interaction force thus obtained accounts *simultaneously* for the geometrical curvature effects (through the GF tensor) and the finite absorption and dissipation of each CNT (through their dielectric response).

To determine $\varepsilon_{zz}(\boldsymbol{R}_{1,2},\omega)$ (and σ_{zz}, accordingly), we first calculate each CNT energy bandstructure using the nearest neighbor tight binding model. Then, the random-phase approximation (RPA) is applied to find the chirality dependent dielectric response with the electronic dissipation processes taken into account in the relaxation time approximation. The RPA model used to calculate CNT optical response can be found in several references[22,23], and here we utilize it with parameters taken from Ref. [17]. Such an approach is known to reproduce reasonably well the optical spectra of CNTs with larger diameters (> 1 nm), where electron-electron correlations and curvature induced inter-tube

hybridization[23] seem to be less significant. The dielectric function is decomposed into a Drude part and a part originating from (transversely quantized) interband electronic transitions $\varepsilon_{zz} = \varepsilon_{zz}^{D} + \varepsilon_{zz}^{inter}$.

We compare our results with the case of infinitely conducting parallel plates. We take the limit $\sigma^{(1,2)} \to \infty$, $R_{1,2} \to \infty$ while keeping $R_1 - R_2 = d$ and find

$$
\begin{aligned}
F = &-\frac{\hbar c}{16\pi^2 R_1^4}\int x_1 dx_1 \sum_{n=0}^{\infty}{}' \frac{(2-\delta_n^0)}{I_n(x_1)K_n(x_2) - I_n(x_2)K_n(x_1)} \\
&\times\left\{\left[x_1^2 K'^2_n(x_1) + \left(n^2 + x_1^2\right)K_n^2(x_1)\right]\times\left[\frac{I_n^2(x_1)K_n(x_2)}{K_n(x_1)} - 2I_n(x_1)I_n(x_2)\right]\right. \\
&-\left[x_1^2 I'^2_n(x_1) + \left(n^2 + x_1^2\right)I_n^2(x_1)\right]\times K_n(x_1)K_n(x_2) \\
&\left.-2\left[x_1^2 I'_n(x_1)K'_n(x_1) + \left(n^2 + x_1^2\right)I_n(x_1)K_n(x_1)\right]I_n(x_2)K_n(x_1)\right\}
\end{aligned}
\tag{8}
$$

where $x_{1,2} = xR_{1,2}$, $I_n(x)$ and $K_n(x)$ are the modified Bessel functions of the first and second kind, respectively. Eq. (8) is obtained by making the transition to imaginary frequencies $\omega \to i\omega$, and using the Euclidean rotation technique as described in Ref. [21]. This can be evaluated by summing the series using the large-order Bessel function expansions[24]. The result is $F \sim (-1/3)(\hbar c\pi^2/240d^4)$, which is about 1/3 of the well-known result for two parallel plates[7]. This deviation originates from $\varepsilon_{zz} \neq 0$ only in our uniaxial model for the CNT dielectric response.

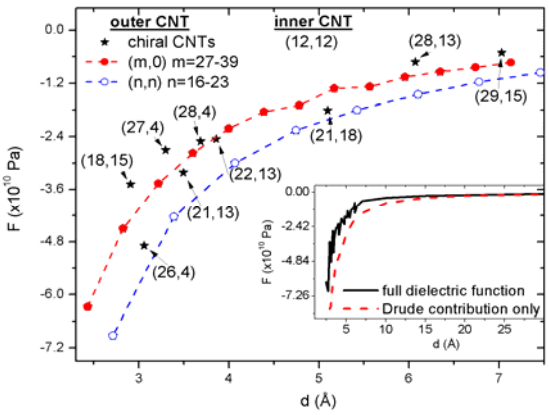

FIG. 2. The Casimir force per unit area as a function of the inter-tube separation *d*, for different pairs of CNTs. The inset shows force found with the full dielectric function and the Drude contribution only for the same CNT pairs indicated in the figure.

To illustrate numerically the inter-tube interaction, we have chosen the inner CNT to be the achiral (12,12) metallic nanotube, and to change the outer tubes. Thus one can envision concentric CNTs consisting of metal/metal or metal/semiconductor combinations of different chiralities but of similar radial dimensions. Fig. 2 shows that *F* decreases in strength as the tube separation increases. This dependence is monotonic for the zigzag (*m*,0) and armchair (*n*,*n*) outer

tubes, but it happens at different rates. The attraction is stronger for (*n*,*n*) outer CNT as compared to the attraction for the outer (*m*,0) ones. For chiral tubes *F* decreases as a function of *d* in a rather irregular fashion. It is seen that for relatively small *d*, the force can be quite different. For example, the attraction between (27,4)@(12,12) and (21,13)@(12,12) differ by ~20% in favor of the second pair, even though the radial difference is only 0.2 Å. The difference becomes smaller as the CNTs separation becomes larger, and they eventually become negligible as the force diminishes at large distances.

We also calculate the force using the ε_{zz}^{D} contribution alone in each dielectric function. The inset in Fig.2 indicates that *F* is stronger when the interband transitions are neglected. The decay of *F* vs. *d* is monotonic. Including the ε_{zz}^{inter} term reduces the force at different rates due to the chirality dependent interband electronic transitions. At large separations, the discrepancies between the force calculated with the full dielectric response, and those obtained with the Drude term only become less significant. We find that for *d*~15 Å, this difference is less than 10%.

To investigate further the important functionalities originating from the cylindrical geometry and the CNT dielectric response properties, *F* is calculated for different achiral inner/outer nanotube pairs. Studying zigzag and armchair CNTs allows tracking generalities from $\varepsilon(\omega)$ in a more controlled manner. The results are presented in Fig. 3. We have chosen representatives of three inner CNT types – metallic (12,12), semi-metallic (21,0), and semiconducting (20,0) nanotubes. They are of similar radii, 8.14 Å, 8.22 Å and 7.83 Å, respectively. We see that depending on the outer nanotube types, the *F* vs *d* curves are positioned in three groups. The weakest interaction is found when there are two zigzag concentric CNTs (top two curves). The fact that some of these are semi-metallic and others are semiconducting does not seem to influence the magnitude and monotonic decrease of the force. The attraction is stronger when there is a combination of an armchair and a zigzag CNT as compared to the previous case. The curves for (*m*,0)@(12,12), (*n*,*n*)@(21,0), and (*n*,*n*)@(20,0) are practically overlapping, meaning that the specific location of the zigzag and armchair tubes (inner or outer) is of no

significance to the force. The small deviations can be attributed to the small differences in the inner CNT radii. Finally, we see that the strongest interaction occurs between two armchair CNTs (red curve). These functionalities are not unique just for the considered CNTs. We have performed the same calculations for many different tubes, and we always find that the strongest interaction occurs between two armchair CNTs and the weakest – between two zigzag CNTs (provided that their radial dimensions are similar).

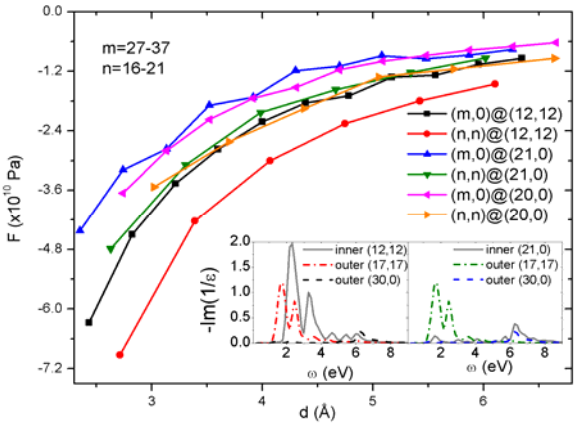

FIG. 3. The Casimir force per unit area as a function of the inter-tube separation *d* for selected tube pairs. The insets show the EELS spectra for several CNTs.

The results from these calculations show that the CNT collective excitation properties have a strong effect on their mutual interaction. This is particularly true for the relatively small distances of interest here, for which the dominant contribution of plasmonic modes to the Casimir interactions has been realized for planar[25,26] and linear[27] metallic systems. To elucidate this issue here, we calculate the Electron Energy Loss Spectroscopy (EELS) spectra, given by $\mathrm{Im}\left[-1/\varepsilon(\omega)\right]$, using the RPA model[17], and compare them for various inner and outer CNTs combinations – Fig. 3 (inset). The peaks in EELS are interpreted as collective plasmon excitations originating from interband transitions between the Brillouin zone van Hove singularities of each CNT[1,28].

Considering *F* as a function of *d* and the specific form of the EELS spectra, it becomes clear from the inset in Fig.3 that the low frequency excitations, given by peaks in $\mathrm{Im}\left[-1/\varepsilon(\omega)\right]$, are key to the strength of the inter-tube interaction. We always find that the strongest force is between the CNTs with well pronounced overlapping low frequency peaks. This is consistent with the conclusion of Ref. [27] for generic 1D-plasmonic structures. However, in our case we deal with the interband plasmons originating from the space quantization of the transverse electronic motion, and, therefore, having quite a different

frequency-momentum dispersion law (constant) as compared to that normally assumed (linear) for plasmons[29]. A weaker force is obtained if only one of the CNTs supports strong low frequency interband transitions. The weakest interaction happens when neither CNT has strong low frequency peaks in EELS. For the cases shown in Fig.3, one finds well pronounced overlapping transitions in the (12,12) CNT at ω_1=2.18 eV and ω_2=3.27 eV, and at ω_1=1.63 eV and ω_2=2.45 eV in the (17,17) CNT. At the same time, no such well defined strong low frequency excitations in the (21,0) and (30,0) CNTs are found. Fig. 3 shows that the attraction in (17,17)@(12,12) is much stronger than the attraction in (30,0)@(21,0), even though the radial sizes of the involved CNTs are approximately the same. One also notes that for the case of (17,17)@(21,0) there is only one such low frequency excitation coming from the armchair tube, and consequently the force has an intermediate value as compared to the above discussed two cases.

We performed calculations of the interaction force between many CNT pairs and made comparisons between the relevant regions of the EELS spectra. It is found that, in general, armchair tubes always have strong, well pronounced interband excitations in the low frequency range. Zigzag and most chiral CNTs have low frequency interband transitions[4], too, but they are not as near as well pronounced as those in armchair tubes; their stronger excitations are found at higher frequencies.

We further investigate how the collective excitations from the EELS spectra influence the interaction by considering two concentric cylinders with radii R_1=11.63 Å and R_2=8.22 Å. The dielectric function of each cylinder is taken to be of the generic Lorentzian form $\varepsilon(R_{1,2},\omega)=1-\Omega^2/(\omega^2-\omega_{1,2}^2+i\omega\Gamma)$ with Ω=2.7 eV and Γ=0.03 eV. Then, the EELS spectrum has only one resonance at $\omega_{1,2}$ for each cylinder. This generic form allows us to change the relative position and strength of the peaks and uncover more characteristic features originating from the EELS spectra. In Fig. 4, the force as a function of the peak frequency of the outer cylinder is shown when the frequency for the inner cylinder is kept constant (four values are chosen for ω_2). One sees that the local minima in F vs ω occur when ω_1 and ω_2 coincide. In

fact, the strongest attraction happens when the structure has the lowest excitations at the same frequency $\omega_1 = \omega_2 = 0.81$ eV. It is evident that the existence of relatively strong low frequency EELS spectrum *and* an overlap between the relevant peaks of the two structures is necessary to achieve a strong interaction.

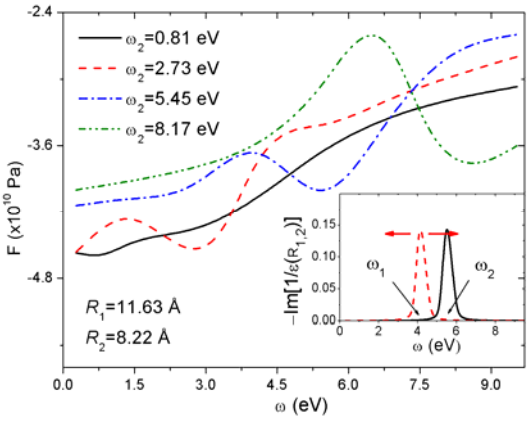

FIG. 4. The Casimir force per unit area as a function of the frequency of the peak in EELS of the outer cylinder, while the inner cylinder peak frequency ω_2 is constant. Results are shown for four values of ω_2. The dielectric functions are modeled by a generic Lorentzian.

This study clearly demonstrates the crucial importance of the collective low energy surface plasmon excitations along with the cylindrical geometry for the long-ranged interaction in a double wall CNT system. The presented approach provides the unique opportunity to investigate these features together and to uncover underlying mechanisms of the energetic stability of different double wall CNT combinations. Our results are in good agreement with experimental measurements on determining the chirality of individual double wall CNTs. Electron diffraction methods[6] have shown that the chiral spectrum of nanotubes with average size distributions has displayed a tendency for both the inner and outer tubes to be of armchair type. Thus our results may be viewed as describing one of the possible reasons for the preference of having a double wall CNT formed by two armchair ones.

In summary, we have applied a QED approach to study the interaction between concentric CNTs with the realistic dielectric response taken into account. We found that at distances similar to the equilibrium separations between graphitic surfaces the attraction is dominated by the low energy (interband) plasmon excitations of both CNTs. The key attributes of the EELS spectra resulting in the strongest interaction are the existence of low frequency transitions, their strong and well pronounced nature, and the overlap between the low frequency peaks belonging to the two CNTs. Thus, we have shown that the

collective surface excitations and their chirality dependent characteristics play a profound role in the interaction strength in double wall CNT systems.

We acknowledge financial support under contract DE-FG02-06ER46297. I. V. B. is supported by NSF, ARO and NASA (grants HRD-0833184, W911NF-10-1-0105, and NNX09AV07A).

REFERENCES

[1] R. Saito, G. Dresselhaus, and M. S. Dresselhaus, *Physical Properties of Carbon Nanotubes* (Imperial College Press, London, 1998).

[2] R. Fermani, S. Scheel, and P. L. Knight, Phys. Rev. A 75, 062905 (2007).

[3] I. V. Bondarev and B. Vlahovic, Phys. Rev. B 75, 033402 (2007).

[4] I. V. Bondarev, L. M. Woods, and K. Tatur, Phys. Rev. B 80, 085407 (2009)

[5] A. Popescu, L. M. Woods, and I. V. Bondarev, Nanotechnology 19, 435702 (2008); A. Popescu and L. M. Woods, Appl. Phys. Lett. 95, 203507 (2009).

[6] K. Hirahara et al, Phys. Rev. B 73, 195420 (2006); M. Kociak et al, Phys. Rev. Lett. 89, 155501 (2002).

[7] H. B. G. Casimir, Proc. K. Ned. Akad. Wet. 51, 793 (1948).

[8] M. J. Sparnaay, Physica 24, 751 (1958).

[9] S. K. Lamoreaux, Phys. Rev. Lett. 78, 5 (1997) ; U. Mohideen and A. Roy, Phys. Rev. Lett. 81, 4549 (1998); F. Chen and U. Mohideen, Rev. Sci. Instrum. 72, 3100 (2001).

[10] M. Bordag, U. Mohideen, and V. M. Mostepanenko, Phys. Rep. 353, 1 (2001).

[11] V. A. Parsegian, *van der Waals forces* (Cambridge University Press, Cambridge, 2005).

[12] R. F. Rajter et al, Phys. Rev. B 76, 045417 (2007).

[13] M. Bordag, B. Geyer, G. L. Klimchitskaya, and V. M. Mostepanenko, Phys. Rev. Lett. 85, 503 (2000); G. L. Klimchitskaya, U. Mohideen, and V. M. Mostepanenko, Rev. Mod. Phys. 81, 1827 (2009).

[14] S. Y. Buhmann and D. G. Welsch, Prog. Quantum Electron. 31, 51 (2007).

[15] J. Peng, J. Wu, K. C. Hwang, J. Song, and Y. Huang, J. Mech. Phys. Solids 56, 2213 (2008).

[16] Y. Huang, J. Wu, and K. C. Hwang, Phys. Rev. B 74, 245413 (2006).

[17] S. Tasaki, K. Maekawa, and T. Yamabe, Phys. Rev. B 57, 9301 (1998).

[18] V. N. Popov and L. Henrard, Phys. Rev. B 70, 115407 (2004); A. G. Marinopoulos, L. Reining, A. Rubio, and N. Vast, Phys. Rev. Lett. 91, 046402 (2003); L X. Benedict, S. G. Louie, and M. L. Cohen, Phys. Rev. B 52, 8541 (1995); Z. M. Li et al, Phys. Rev. Lett. 87, 127401 (2001).

[19] I. V. Bondarev, G. Ya. Slepyan, and S. A. Maksimenko, Phys. Rev. Lett. 89, 115504 (2002).

[20] C. T. Tai, *Dyadic Green Functions in Electromagnetic Theory*, 2nd Ed. (IEEE Press, Piscatawnay, NY, 1994); L. W. Li, M. S. Leong, T. S. Yeo, and P. S. Kooi, J. Electr. Waves Appl. 14, 961 (2000).

[21] I. Cavero-Pelaez and K. A. Milton, Annals of Phys. 320, 108 (2005); K. A. Milton, L. L. DeRaad Jr., and J. Schwinger, Ann. Phys. 115, 388 (1978).

[22] W. A. Harrison, *Electronic Structure and the Properties of Solids* (Freeman, San Francisco, 1980);

[23] J. C. Charlier, X. Blase, and S. Roche, Rev. Mod. Phys. 79, 677 (2007); M. F. Lin and K. W. K. Shung, Phys. Rev. B 50, 17744 (1994); V. Zolyoni et al, Phys. Rev. B 77, 245403 (2008).

[24] *Handbook of Mathematical Functions*, edited by M. Abramovitz and I. A. Stegun (Dover, NY, 1972).

[25] N. G. van Kampen, B. R. A. Nijboer and K. Schram, Phys. Lett. A 26, 307 (1968).

[26] F. Intravaia and A. Lambrecht, Phys. Rev. Lett. 94, 110404 (2005).

[27] J. F. Dobson, A. White, and A. Rubio, Phys. Rev. Lett. 96, 073201 (2006).

[28] *Plasmons: Theory and Applications*, edited by K. N. Helsey (Nova Science Publishers, NY, 2010).

[29] T. Pichler et al, Phys. Rev. Lett., 80, 4729 (1998).